Combination of UAV and terrestrial photogrammetry to assess rapid glacier evolution and map glacier hazards

Fugazza, Davide[1]; Scaioni, Marco[2]; Corti, Manuel[2]; D'Agata, Carlo[3]; Azzoni, Roberto Sergio[3]; Cernuschi, Massimo[4]; Smiraglia, Claudio[1]; Diolaiuti, Guglielmina Adele[3]

[1]Department of Earth Sciences 'A.Desio', Università degli studi di Milano, 20133 Milano Italy

[2]Department of Architecture, Built Environment and Construction Engineering, Politecnico di Milano, 20133 Milano Italy

[3]Department of Environmental science and policy (DESP), Università degli studi di Milano, 20133 Milano Italy

[4]Agricola 2000 S.C.P.A., 20067 Tribiano (MI) Italy

Correspondence to: Marco Scaioni (marco.scaioni@polimi.it)

Abstract

Tourists and hikers visiting glaciers all year round face hazards such as the rapid formation of collapses at the terminus, typical of such a dynamically evolving environment. In this study, we analysed the potential of different survey techniques to analyze hazards of the Forni glacier, an important geo-site located in Stelvio Park (Italian Alps). We carried out surveys in the ablation season 2016 and compared point clouds generated from UAV, close range photogrammetry and terrestrial laser scanning (TLS). To investigate the evolution of glacier hazards and evaluate the glacier thinning rate, we also used UAV data collected in 2014 and a DEM from an aerial photogrammetric survey of 2007. We found that the integration between terrestrial and UAV photogrammetry is ideal to map hazards related to the glacier collapse, while TLS is affected by occlusions and logistically complex in glacial terrain. Photogrammetric techniques can therefore replace TLS for glacier studies and UAV-based DEMs hold potential to become a standard tool to investigate the glacier geodetic mass balance. Based on our datasets, an increase in the size of collapses was found over the study period, and the glacier thinning rates went from 4.55 ± 0.24 ma^{-1} between 2007 and 2014 to 5.20 ± 1.11 ma^{-1} between 2014 and 2016.

1 Introduction

Glacier and permafrost-related hazards can be a serious threat to humans and infrastructure in high mountain regions (Carey et al., 2014). The most catastrophic cryospheric hazards are generally related to the outburst of water, either through breaching of moraine- or ice-dammed lakes or from the englacial or subglacial system, causing floods and debris flows. Ice avalanches from hanging glaciers can also have serious consequences for downstream populations (Vincent et al., 2015), as well as debris flows caused by the mobilization of accumulated loose sediment on steep slopes (Kaab et al., 2005a). Less severe hazards, but still particularly threatening for mountaineers are the detachment of seracs (Riccardi et al., 2010) or the collapse of ice cavities (Gagliardini et al., 2011; Azzoni et al., submitted). While these processes are in part typical of glacial and periglacial environments, there is evidence that climate change is increasing the likelihood of specific hazards (Kaab et al., 2005a). In the European Alps, accelerated formation and growth of proglacial moraine-dammed lakes has been reported in Switzerland, amongst concern of possible overtopping of moraine dams provoked by ice avalanches (Gobiet et al., 2014). Ice avalanches themselves can be more frequent as basal sliding is enhanced by the abundance of meltwater in warmer summers (Clague, 2013). Glacier and permafrost retreat, which have been reported in all sectors of the Alps (Smiraglia et al., 2015; Fischer et al., 2014; Gardent et al, 2014; Harris et al., 2009), are a major cause of slope instabilities which can result in debris flows, by debuttressing rock and debris flanks and promoting the exposure of unconsolidated and ice-cored sediments (Keiler et al., 2010; Chiarle et al., 2007). Glacier downwasting is also increasing the occurrence of structural collapses and while not directly threatening human lives, sustained negative glacier mass balance can also cause shortages of water for industrial, agricultural and domestic use and energy production, affecting even populations living away from glaciers. Finally, glacier retreat and the increase in glacier hazards negatively influence the tourism sector and the economic prosperity of high mountain regions (Palomo, 2017).

The increasing threat from cryospheric hazards under climate change calls for the adoption of mitigation strategies. Remote Sensing has long been recognized as an important tool to produce supporting data to this purpose, owing to the ability to generate digital elevation models (DEMs) and multispectral images. DEMs are particularly useful to detect glacier thickness and volume variations (Fischer et al., 2015; Berthier et al., 2016) and to identify steep areas that are most prone to geomorphodynamic changes such as mass movements (Blasone et al., 2014). Multispectral images at a sufficient spatial resolution enable the recognition of most cryospheric hazards (Quincey et al, 2005; Kaab et al., 2005b). While satellite images from Landsat and ASTER sensors (15-30 m ground sample distance - GSD) are practical for regional-scale mapping (Rounce et al, 2017), the assessment of hazards at the scale of individual glaciers or basins requires higher spatial resolution, which in the past could only be achieved via dedicated field campaigns with terrestrial laser scanners (TLS) (Kellerer-Pirklbauer et al., 2005; Riccardi et al., 2010). Recent years have seen a resurgence of terrestrial photogrammetric surveys for the generation of DEMs (Piermattei et al., 2015, 2016; Kaufmann and Seier, 2016) due to important technological advancements including the development of Structure-from-Motion (SfM) Photogrammetry and its implementation in fully automatic processing software, as well as the improvements in the quality of camera sensors (Eltner et al., 2016; Westoby et al., 2012). In parallel, unmanned aerial vehicles (UAVs – Colomina & Molina, 2014, O’Connor et al., 2017) have started to emerge as a viable alternative to TLS for multi-temporal monitoring of small areas. UAVs promise to bridge the gap between field observations, notoriously difficult on glaciers, and coarser resolution satellite data (Bhardwaj et al., 2016). Although the number of studies employing them in high mountain environments is slowly increasing (see e.g. Fugazza et al., 2015; Gindraux et al., 2017; Seier et al, 2017), their full potential for monitoring of glaciers and particularly glacier hazards has still to be explored. In particular, the advantages of UAV and terrestrial SfM-Photogrammetry, and the possibility of data fusion to support hazard management strategies in glacial environments needs to be investigated and assessed.

In this study, we investigated a rapidly downwasting glacier in a protected area and highly touristic sector of the Italian Alps, Stelvio National Park. We focused on the glacier terminus and the hazards identified there, i.e., the formation of normal faults and ring faults. The former occur mainly on the medial moraines and glacier terminus and are due to gravitational collapse of debris-laden slopes. The latter develop as a series of circular or semicircular fractures with stepwise subsidence, caused by englacial or subglacial meltwater creating voids at the ice-bedrock interface and eventually the collapse of cavity roofs. While often overlooked, these collapse structures are particularly hazardous for mountaineers and likely to increase under a climate change scenario (Azzoni et al., submitted). They are more dangerous than crevasses because of the larger size and because they could be filled with snow and rendered entirely or partly invisible to mountaineers.

We conducted our first UAV survey of the glacier in 2014; then, through a dedicated field campaign carried out in summer 2016, we compared different platforms and techniques for point cloud, DEM and orthomosaic generation to assess their ability to monitor glacier hazards: UAV photogrammetry, terrestrial photogrammetry and TLS. The aims were: (1) comparing UAV- and terrestrial photogrammetric products acquired in 2016 against the TLS point cloud; (2) identifying glacier-related hazards and their evolution between 2014-2016 using the merged point cloud from UAV and terrestrial photogrammetry and UAV orthophotos; and 3) investigating ice thickness changes between 2014-2016 and 2007-2016 by comparing the two UAV DEMs and a third DEM obtained from stereo-processing of aerial photos captured in 2007.

2 Study Area

The Forni Glacier (see Fig. 1) has an area of 11.34 km^2 based on the 2007 data from the Italian Glacier Inventory (Smiraglia et al., 2015), an altitudinal range between 2501 and 3673 m a.s.l. and a North-North-Westerly aspect. The glacier retreated markedly since the little ice age (LIA), when its area was 17.80 km^2 (Diolaiuti & Smiraglia, 2010), with an acceleration of the shrinking rate in the last three decades, typical of valley glaciers in the Alps (Diolaiuti et al., 2012, D'Agata et al.; 2014). It has also undergone profound changes in dynamics in recent years, including the loss of ice flow from the eastern accumulation basin towards its tongue and the evidence of collapsing areas on the eastern tongue (Azzoni et al., submitted). One such area, hosting a large ring fault (see Fig. 2d) prompted an investigation carried out with Ground Penetrating Radar (GPR) in October 2015, but little evidence of a meltwater pocket was found under the ice surface (Fioletti et al., 2016). Since then, a new ring fault appeared on the central tongue, and the terminus underwent substantial collapse (see Fig. 2a,b,c,e). Continuous monitoring of these hazards is important as the site is highly touristic (Garavaglia et al., 2012), owing to its location in Stelvio Park, one of Italy's major protected areas, and its inclusion in the list of geosites of Lombardy region (see Diolaiuti and Smiraglia, 2010). The glacier is in fact frequently visited during both summer and winter months. During the summer, hikers heading to Mount San Matteo take the trail along the central tongue, accessing the glacier through the left flank of the collapsing glacier terminus. During wintertime, ski-mountaineers instead access the glacier from the eastern side, crossing the medial moraine and potentially collapsed areas there (see Fig. 1).

3 Data Sources: acquisition and processing

3.1 UAV Photogrammetry

3.1.1 2014 Dataset

The first UAV survey took place on 28th August 2014, using a SwingletCam fixed wing aircraft (see Fig. 3a). This commercial platform developed by SenseFly carries a Canon Ixus 127 HS compact digital camera. The UAV was flown in autopilot mode with a relative flying height of approximately 380 m above the glacier surface, which resulted in an average GSD of 12 cm. The flight plan was organized by using the proprietary software eMotion, by which the aircraft follows predefined waypoints with a nominal along-strip overlap of 70%; sidelap was not regular because of the varying surface topography, but was approximately 60%. Flight operations started at 07:44 AM and ended at 08:22 AM. Early morning operations were preferred to avoid saturating camera pictures, as during this time of day the glacier is not yet directly illuminated by the sun, and to minimize blurring effects due to the UAV motion, since wind speed is at its lowest on glaciers during morning hours (Fugazza et al., 2015). Pictures were automatically captured by the UAV platform, selecting the best combination of sensor aperture (F=2.7), sensitivity (between 100-400 ISO) and shutter speed (between 1/125 s - 1/640 s). The survey covered an area of 2.21 km^2 in just two flight campaigns, with a low altitude take-off (lake Rosole, close to Branca Hut, see Fig. 1). Both the terminal parts of the central and eastern ablation tongue were surveyed.

Processing of data from the 2014 UAV flight was carried out using Agisoft Photoscan version 1.2.4 (www.agistoft.com), implementing a SfM algorithm for image orientation (Spetsakis and Aloimonos, 1991) followed by a multi-view dense-matching approach for surface 3D reconstruction (Furukawa and Ponce, 2009). Since no GCPs were measured during the 2014 campaign, the registration of this data set into the mapping reference system was based on GNSS (Global Navigation Satellite System) navigation data only. Consequently, a global bias in the order of 1.5-2 m resulted after geo-referencing, and no control on the intrinsic geometric block stability could be possible. After the generation of the point cloud, a DEM and orthoimage were produced using the method described by Immerzeel et al. (2014), with spatial resolutions of 60 cm and 15 cm, respectively.

3.1.2 2016 Dataset

The two UAV surveys were carried out on 30th August and 1st September 2016, both around midday with 8/8 of the sky covered by stratocumulus clouds. The UAV employed in these surveys was a customized quadcopter (see Fig. 3b) carrying a Canon Powershot 16 Megapixel digital camera. Two different take-off and landing sites were chosen to gain altitude before take-off and maintain line-of-sight operation with a flying altitude of 50 m above ground, which ensured an average ground sample distance (GSD) of 6 cm. The first take-off site was on the eastern lateral moraine (elevation approx.

2700 m a.s.l.), while the second site was a rock outcrop on the hydrographic left flank of the glacier (see Fig. 1) at an elevation of approx. 2750 m a.s.l. To reduce motion blur, camera shutter speed was set to the lowest possible setting, 1/2000 s, with aperture at F/2.7 and sensitivity at 200 ISO.

Several individual parallel flights were conducted to cover a small section of the proglacial plain and different surface types on the glacier surface, including the terminus, a collapsed area on the central tongue, the eastern medial moraine and some debris-covered parts of the eastern tongue. A ‘zig-zag’ flying scheme was followed to reduce the flight time. The UAV was flown in autopilot mode using the open-source software Mission Planner (Oborne, 2013) to ensure 70% along-strip overlap and sidelap. In total, two flights were performed during the first survey and three during the second, lasting about 20 minutes each. The surveyed area spanned over 0.59 km^2.

Processing of data from the 2016 UAV flight was carried out using Agisoft Photoscan version 1.2.4. Eight GCPs (see Fig. 1) were measured for the registration of the photogrammetric blocks and its by-products into the mapping system. The root mean square error (RMSE) of the GCPs was 40 cm, which can be used as an indicator of accuracy for the geo-referencing of the photogrammetric block. The point cloud obtained from the 2016 UAV flight was interpolated to produce a DEM and orthoimage with the same cell resolution as the 2014 dataset, i.e., 60 and 15 cm, respectively. Both products were exported in the ITRS2000 / UTM 32N mapping reference system.

3.2 Terrestrial photogrammetry

The terrestrial photogrammetric survey was carried out during on 29th August 2016 to reconstruct the topographic surface of the glacier terminus, which presented several vertical and subvertical surfaces whose measurement was not possible from the UAV platform carrying a camera in nadir configuration (see Fig. 2e).

Images were captured from 134 ground-based stations, most of them located in front of the glacier, and some on both flanks of the valley in the downstream area, as shown in Fig. 4a. A single-lens-reflex Nikon D700 camera was used, equipped with a 50 mm lens, and a full-frame CMOS sensor (36x24 mm) with 4256x2823 pixels. This photogrammetric block was processed using Agisoft Photoscan version 1.2.4. In this case, since no preliminary information about approximate camera position was collected, the SfM procedure was run without any initial information.

Seven natural features visible on the glacier front were used as GCPs to be included in the bundle adjustment computation in Agisoft Photoscan. Measurement of GCPs in the field was carried out by means of a high-precision theodolite. The measurement of points previously recorded with a GNSS geodetic receiver allowed to register the coordinates of GCPs in the mapping reference system. The RMSE of 3D residual vectors on GCPs was 34 cm, which can be considered as the accuracy of absolute geo-referencing. The final point cloud obtained from the dense matching tool implemented in Agisoft Photoscan covers at a very high spatial resolution the full glacier terminus, with the exception of a few obstructed parts (see Fig. 4b).

3.3 Terrestrial Laser Scanning

On the same days as the first UAV survey of 2016, a long-range terrestrial laser scanner Riegl LMS-Z420i was used to scan the glacier terminus frontally. One instrumental standpoint located on the hydrographic left flank of the glacier terminus (see Fig. 1) was established. The horizontal and vertical scanning resolution were set up to provide a spatial point density of approx. 5 cm on the ice surface at the terminus. Geo-referencing was accomplished by placing five GCPs consisting in cylinders covered by retroreflective paper. The coordinates of GCPs were measured by using a precision theodolite following the same procedure adopted for terrestrial photogrammetry. Considering the accuracy of registration and the expected precision of laser point measurement, the global accuracy of 3D points was estimated in the order of ±7.5 cm.

3.4 GNSS ground control points

Prior to the 2016 surveys, eight control targets were placed both outside the glacier and on the glacier tongue (see Fig. 1). Differential GNSS data were acquired at their location for accurate geo-referencing of UAV, terrestrial photogrammetry and TLS data. While for geo-referencing of UAV data the GCPs were directly visible on the quadcopter images, for terrestrial photogrammetry and TLS they were adopted for the registration of theodolite measurements. The targets consisted in a piece of white fabric 80 x 80 cm wide, with a circular marker in red paint chosen to provide contrast against the background. Except for the one GCP located at the highest site, such GCPs were positioned on large, flat boulders to provide a stable support and reduce the impact of ice ablation between flights.

GNSS data were acquired by means of a pair of Leica Geosystems 1200 geodetic receivers working in RTK (Real-Time Kinematics) mode (see Hoffman-Wellenhof, 2008). One of them was set up as master on a boulder beside Branca Hut, where a monument had been established with known coordinates in the mapping reference system ITRS2000 / UTM 32N. The second receiver was used as a rover, communicating via radio link with the master station. The maximum distance between master and rover was less than 1.5 km, but the local topography prevented broadcasting the differential corrections in a few zones of the glacier. Unfortunately, no mobile phone services were available and consequently the internet network could not be accessed, precluding the use of the regional GNSS real-time positioning service. Non-RTK points were processed in fast-static mode, requiring a longer measurement time of approx. 12 minutes. The theoretical accuracy of GCPs was estimated in the order of 2-3 cm.

3.5 2007 DEM

The 2007 TerraItaly DEM was produced by BLOM C.G.R. company for Lombardy region. It is the final product of an aerial survey over the entire region,that was conducted with a multispectral pushbroom Leica ADS40 sensor acquiring images from a flying height of 6,300 m with an average GSD of 65 cm. The images were processed to generate a DEM with a cell resolution of 2 m x 2 m, and projected in the former national 'Gauss Boaga - Fuso I' mapping reference system based on Monte Mario datum (Mugnier, 2005). Heights were converted from ellipsoidal to geodetic using the official software for datum transformation in Italy (Verto ver. 3), which is distributed by the Italian Geographic Military Institute (IGMI). The final vertical accuracy reported by BLOM C.G.R. is ± 3 m. The only processing step performed within this study was the datum conversion to ITRS2000, using a seven-parameter similarity transformation based on a local parameter set provided by IGMI.

4 Methods

4.1 Analysis of point clouds from the 2016 campaign: UAV/terrestrial photogrammetry and TLS

The comparison between point clouds generated during the 2016 campaign had the aim of assessing their geometric quality before their application for the analysis of hazards. These evaluations were also expected to provide some guidelines for the organization of future investigations in the field at the Forni Glacier and in other Alpine sites. Specifically, we analysed point density (points/m^2) and completeness, i.e. % of area in the ray view angle. Point density partly depends upon the adopted surveying technique, since it is controlled by the distance between sensor and surface and the obtainable spatial resolution. In SfM-Photogrammetry, the latter property is affected by dense matching, while in TLS it can be set up as data acquisition input parameter. In this study, the number of neighbours N (inside a sphere of radius R=1 meter) divided by the neighbourhood surface was used to evaluate the local point density D in CloudCompare (www.cloudcompare.org). To understand the effect of point density dispersion (Teunissen, 2009), the inferior 12.5 percentile of the standard deviation σ of point density was also calculated. The use of these local metrics allowed to distinguish between point density in different areas, since this may largely change from one portion of surface to another. A further metric in this sense was point cloud completeness, referring to the presence of enough points to completely describe a portion of surface. In this study, the visual inspection of selected sample locations was used to identify occlusions and areas with lower point density.

To analyse these properties, five regions were selected (see Fig. 5), located on the glacier topographic surface and characterized by different glacier features and the presence of hazards: 1) Glacial cavity composed by subvertical and fractured surfaces over 20 m high, and forming a typical semicircular shape; 2) glacial cavity over 10 m high with the same typical semi-circular shape as location 1, covered by fine- and medium-size rock debris; 3) normal fault over 10 m high; 4) highly-collapsed area covered by fine- and medium-size rock debris and rock boulders; and 5) planar surface with a normal fault covered by fine- and medium-size rock debris and rock boulders. The analysis of local regions was preferred to the analysis of the entire point clouds for the following reasons: 1) the incomplete overlap between point clouds obtained from different methods; 2) the opportunity to investigate the performances of the techniques in diverse geomorphological situations.

Finally, we compared the point clouds in a pairwise manner within the same sample locations. Since no available benchmarking data set (e.g. accurate static GNSS data) was concurrently collected during the 2016 campaign, the TLS point cloud was used as a reference, as it less influenced by controlling factors (network geometry, object texture, lighting conditions). When comparing both photogrammetric data sets, the one obtained from UAV was used as reference because of the even distribution of point density within the sample locations. The presence of residual, non-homogenous geo-referencing errors in the data sets required a specific fine registration of each individual sample location, which was conducted in CloudCompare using the ICP algorithm (Pomerleau et al., 2016). Then, point clouds in corresponding sample areas were compared using the M3C2 algorithm implemented in CloudCompare (Lague et al., 2013). This solution allowed us to get rid of registration errors from the analysis, which could then be focused on the capability of the adopted techniques to reconstruct the local geometric surface of the glacier in an accurate way.

4.2 Merging of UAV and close-range photogrammetric point clouds

To improve coverage of different glacier surfaces, including planar areas and normal faults, photogrammetric point clouds from the 2016 campaign were merged. Prior to point cloud merging, a preliminary co-registration was performed on the basis of the ICP algorithm in CloudCompare. Regions common to both point clouds were used to minimize the distances between them and find the best co-registration. The point cloud from UAV photogrammetry, which featured the largest extension, was used as reference during co-registration, while the other was rigidly transformed to fit with it. After this task, both original point clouds resulted aligned into the same reference system. In order to get rid of redundant points and to obtain a homogenous point density, the merged point cloud (see Fig. 5) was subsampled keeping a minimum distance between adjacent points of 20 cm. The final size of this data set is approximately 4.4 million points, which represents a manageable data amount on up-to-date computers. The colour RGB information associated to each point in the final point cloud was derived by averaging the RGB information of original points in the subsampling volumes. While this operation resulted in losing part of the original RGB information, it helped provide a realistic visualization of the topographic model, which can aid the interpretation of glacier hazards.

4.2 Glacier hazard mapping

The investigation of glacier hazards was conducted by considering datasets from 2014 and 2016. In 2014, only the point cloud and UAV orthophoto were available, while in 2016 the point cloud obtained by merging UAV and close-range photogrammetric data sets was used in combination with the UAV orthophoto. In this study, we focused on ring faults and normal faults, which were manually delineated by using geometric properties from the point clouds while color information from orthophotos was used as a cross-check. On point clouds, mapping is based on visual inspection of vertical displacements following faulting or subsidence. On orthophotos, both types of structures also generally appear as linear features in contrast with their surroundings. As these structures may look similar to crevasses, further information concerning their orientation and location needs to be assessed for discrimination. The orientation of fault structures is not coherent with glacier flow, with ring faults also appearing in circular patterns. Their location is limited to the glacier margins, medial moraines and terminus (Azzoni et al., submitted). After delineation, we also analysed the height of vertical facies using information from the point clouds.

4.3 DEM co-registration for glacier thickness change estimation

Several studies have found that errors in individual DEMs, both in the horizontal and vertical domain, propagate when calculating their difference leading to inaccurate estimations of thickness and volume change (Berthier et al., 2007; Nuth & Kaab, 2011). In the present study, different approaches were adopted for geo-referencing all the DEMs (2007, 2014, 2016) used in the analysis of the volume change of the Forni Glacier tongue. To compute the relative differences between the DEMs, a preliminary co-registration was therefore required. The method proposed by Berthier et al. (2007) for the co-registration of two DEMS was separately applied to each DEM pair (2007-2014; 2007-2016; 2014-2016). Following this method, in each pair one DEM plays as reference ('master'), while the other is used as 'slave' DEM to be iteratively shifted along x and y directions by fractions of pixel to minimize the standard deviation of elevation differences with respect to the ‘master’ DEM. Only areas assumed to be stable are considered in the calculation of the co-registration shift. The ice-covered areas were excluded by overlaying the glacier outlines from D’Agata et al. (2014) for 2007 and Fugazza et al. (2015) for 2014. The oldest DEM, which is also the widest in each comparison, was always set as the master. To co-register the 2014 and 2016 DEMs with the 2007 DEM, both were resampled to 2 m spatial resolution, whereas the comparison between 2014 and 2016 was carried out at the original resolution of these data sets (60 cm).

All points resulting in elevation differences larger than 15 m were labelled as unreliable, and consequently discarded from the subsequent analysis. Such larger discrepancies may denote errors in one of the DEMs or unstable areas outside the glacier. Values exceeding this threshold, however, were only found in a marginal area with low image overlap in the comparison between the 2014 and 2016 DEMs, with a maximum elevation difference of 36 m. Once the final co-registration shifts were computed (see Table 1), the coefficients were subtracted from the top left coordinates of the ‘slave’ DEM; the residual mean elevation difference was also subtracted from the ‘slave’ DEM to bring the mean to zero. After DEM co-registration, the resulting shifts reported in Table 1 were applied to each ‘slave’ DEM, including the entire glacier area. Then the elevations of the ‘slave’ DEM were subtracted from the corresponding elevations of the ‘master’ DEM to obtain the so called DEM of Differences (DoD). Over a reference area common to all three DEMs (Fig. 1), we estimated the volume change and its uncertainty following the method proposed in Howat et al. (2008), which expresses the uncertainty of volume change as the combination of the standard deviation computed from the residual elevation difference over stable areas, and the truncation error implicit when substituting the integral in volume calculation with a finite sum, according to Jokinen and Geist (2010).

5 Results

5.1 Point cloud Analysis

The analysis of point density shows significant differences between the three techniques for point cloud generation (see Table 2). Values range from 103 to 2297 points/m^2 depending on the surveying method, but the density was generally sufficient for the reconstruction of the different surfaces shown in Fig. 5, except for location 5. Terrestrial photogrammetry featured the highest point density, while UAV photogrammetry had the lowest. In relation to UAV photogrammetry, similar point densities were found in all sample locations, especially for the standard deviations that were always in the range 22-29 points/m^2. Mean values were between 103-109 points/m^2 in locations 2-4, while they were higher in location 5 (141 points/m^2). Due to the nadir acquisition points, the 3D modelling of vertical/sub-vertical cliffs in location 1 was not possible. In relation to TLS, a mean value of point density ranging from 141-391 points/m^2 was found, with the only exception of location 5, where no sufficient data were recorded due to the position of this region with respect to the instrumental standpoint. Standard deviations ranged between 69-217 points/m^2, moderately correlated with respective mean values. The analysis of the completeness of surface reconstruction also revealed some issues related to the adopted techniques (see Fig. 6). Specifically, TLS suffered from severe occlusions which prevented acquisition of data in the central part of the sample area, while UAV photogrammetry was able to reconstruct the upper portion of the sample area but not the vertical cliff. Only terrestrial photogrammetry acquired a large number of points in all areas.

In terms of point cloud distance (see Table 3), the comparison between TLS and terrestrial photogrammetry resulted in a high similarity between point clouds, with no large differences between different sample areas. Conversely, the comparison between TLS and UAV photogrammetry and terrestrial and UAV photogrammetry provided significantly worse results, which may be summarized by the RMSEs in the range 21.1-37.7 cm and 20.7-30.4 cm, respectively. The worse values were both obtained in the analysis of location 2, which mostly represents a vertical surface, while the best agreement was found within location 3 which is less inclined. As the UAV flight was geo-referenced on a set of GCPs with an RMSE of 40.5 cm, the ICP co-registration may have not totally compensated the existing bias.

5.2 Glacier-related hazards and risks

The tongue of Forni glacier hosts a variety of hazardous structures. While most collapsed areas are normal faults, two large ring fault systems can be identified: the first, located in the eastern section (see Fig. 2d and 7), covered an area of 25.6×10^3 m^2 and showed surface lowering up to 5 m in 2014. This area was not surveyed in 2016, since field observation did not show evidence of further subsidence. Conversely, the ring fault that only emerged as a few semi-circular fractures in 2014 grew until cavity collapse, with a vertical displacement up to 20 m and further fractures extending south-eastward (see Fig. 2c and 7), thus potentially widening the extent of collapse in the future. Further smaller ring faults were identified in 2014 at the eastern glacier margin. Only one of them was included in the area surveyed in 2016, with further 2 m subsidence and an increase in subparallel fractures.

Normal faults are mostly found on the eastern medial moraine and at the terminus. Between 2014 and 2016, the first developed rapidly in the vertical domain reaching a height of 12 m in 2016. The collapse was even more rapid at the terminus, leading to the formation of three sub-vertical facies, up to 24 m high, while the height of the vault is as low as 10 m. Several fractures also appear in conjunction with the large ring fault located in the central section of the glacier, extending the fracture system to the western glacier margin. It is likely that the terminus will recede along the fault system on the eastern medial moraine and following the ring faults at the eastern and western margins, increasing the occurrence of hazardous phenomena in these areas.

5.3 Glacier Thickness change

The Forni Glacier tongue was affected by substantial thinning throughout the observation period. Between 2007 and 2014, the largest thinning occurred in the eastern section of the glacier tongue, with changes persistently below –30 m, whereas the upper part of the central tongue only thinned by 10/18 m. The greatest ice loss occurred in correspondence with the normal faults localized in small areas at the eastern glacier margin (see Fig. 8a), with local changes generally below -50 m and a minimum of -66.80 m, owing to the formation of a lake. Conversely, between 2014 and 2016 the central and eastern parts of the tongue had similar thinning patterns, with average changes of -10 m. The greatest losses are mainly found in correspondence with normal faults, with a maximum change of -38.71 m at the terminus and local thinning above 25 m on the lower medial moraine. The ring fault at the left margin of the central section of the tongue also shows thinning of 20/26 m. In the absence of faults, little thinning occurred instead on the upper part of the medial moraine, where a thick debris cover shielded ice from ablation, with changes of -2/-5 m (see Fig. 8c). Considering a common reference area (see Fig. 1, table 4), an acceleration of glacier thinning seems to have occurred over recent years over the lower glacier tongue, from -4.55± 0.24 ma^{-1} in 2007-2014 to -5.20± 1.11 ma^{-1} in 2014-2016, also confirmed by the value of -4.76± 0.29 ma^{-1} obtained from the comparison between 2007 and 2016. Looking at the first two DoD, the trend seems to be caused by the increase in collapsing areas (Fig.8a,b).

6 Discussion

The choice of a technique to monitor glacier hazards and the glacier geodetic mass balance can depend on several factors, including the size of the area, the desired spatial resolution and accuracy, logistics and cost. In this study, we focused on spatial metrics, i.e. point density, completeness and distance between point clouds to evaluate the performance of UAV, close-range photogrammetry and TLS in a variety of conditions.

Considering point density, terrestrial photogrammetry resulted in a denser data set than the other techniques. This is mostly motivated by the possibility to acquire data from several stations with this methodology, only depending on the terrain accessibility, reducing the effect of occlusions with a consequently more complete 3D modelling. However, the mean point density achieved when using terrestrial photogrammetry has a large variability both between different sample locations, and inside each location as shown by the standard deviations of D. Point densities related to UAV photogrammetry and TLS are more regular and constant. In the case of UAV photogrammetry, the homogeneity of point density is due to the regular structure of the airborne photogrammetric block. In the case of TLS, the regularity is motivated by the constant angular resolution adopted during scanning. Since any techniques may perform better when the surface to survey is approximately orthogonal to the sensor looking direction, terrestrial photogrammetry is more efficient for reconstructing vertical and subvertical cliffs (Sample areas 1 and 2) and high-sloped surfaces (Sample areas 3 and 4). On the contrary, airborne UAV photogrammetry provided the best results in location 5 which is less inclined and consequently could be well depicted in vertical photos. In general, point clouds from terrestrial photogrammetry provide a better description of the vertical and subvertical parts (see e.g. Winkler et al., 2012), while point clouds obtained from UAV photogrammetry are more suitable to describe the horizontal or sub-horizontal surfaces on the glacier tongue and periglacial area (Seier et al., 2017), unless the camera is tilted to an off-nadir viewpoint (Dewez et al., 2016; Aicardi et al., 2016). Results obtained from photogrammetry based on terrestrial and UAV platforms can thus be retained quite complementary.

In agreement with other studies of vertical rock slopes (e.g. Abellan et al., 2014), we found that the TLS point cloud was affected by occlusions (see e.g. location 2 in Fig. 6). Data acquisition with this platform is in general difficult in regions that are subparallel to the laser beams and in the presence of wet surfaces. Its main disadvantage compared to photogrammetry is however the complexity of instrument transport and setup. In terms of logistics, up to five people were involved in the transportation of the TLS instruments (laser scanner, theodolite, at least two topographic tripods and poles, electric generator and ancillary accessories) while 2 people were required for UAV and close-range photogrammetric surveys. Meteorological conditions and the limited access to unstable areas close to the glacier terminus also prevented the acquisition of TLS data from other viewpoints as done with photogrammetry. Finally, TLS instruments are much more expensive at 70000-100000€ compared to UAVs (3500€ for our platform) and DSLR (Digital Single-Lens Reflex) cameras used in photogrammetry, in the range 500-3500€.

In this study, the uncertainty of the 2016 UAV dataset (40.5 cm RMSE on GCPs and 21.1-37.7 cm RMSE when compared against TLS) was slightly higher than previously reported in high mountain glacial environments (Immerzeel et al., 2014; Gindraux et al, 2017; Seier et al., 2017). Contributing factors might include the sub-optimal distribution and density of GCPs (Gindraux et al., 2017), the delay between the UAV surveys as well as between UAV and other surveys and the lack of coincidence between GCP placement and the UAV flights. This means the UAV photogrammetric reconstruction was affected by ice ablation and glacier flow, which on Forni Glacier range between 3-5 cm day^{-1} (Senese et al., 2012) and 1-4 cm day^{-1}, respectively (Urbini et al., 2017). We thus expect a combined 3-day uncertainty on the 2016 UAV dataset between 10 and 20 cm, and lower on GCPs considering reduced ablation owing to their placement on boulders. A further contribution to the error budget of GCPs might stem from the intrinsic precision of GNSS/theodolite measurements and image resolution. The comparison between close-range photogrammetry and TLS, was less affected by glacier change as data were collected one day apart and the RMSE of 6-10.6 cm is in line with previous findings by Kaufmann and Landstaedter (2008). To improve the accuracy of UAV photogrammetric blocks, a better distribution of GCPs or switching to an RTK system should be considered, while close-range photogrammetry could benefit from measuring a part of the photo-stations as proposed in Forlani et al. (2014), instead of placing GCPs on the glacier surface.

The uncertainty in UAV photogrammetric reconstruction also factored in the relatively high standard deviation still present after the coregistration between DEMs in areas outside the glacier (2.22 m between 2014 and 2016). Another important factor here is the morphology of the coregistration area, i.e. the outwash plain, still subject to changes owing to the inflow of glacier meltwater and sediment reworking. The final accuracy of our UAV photogrammetric products was nevertheless adequate to investigate ice thickness changes over 2 years, while the integration with close-range photogrammetry was required to investigate hazards related to the collapse of the glacier terminus.

We conducted UAV surveys under different meteorological scenarios, and obtained adequate results with early-morning operations with 0/8 cloud cover and midday flights with 8/8 cloud cover. Both scenarios can provide diffuse light conditions allowing to collect pictures suitable for photogrammetric processing, but camera settings need to be carefully adjusted beforehand (O’Connor et al., 2017). If early morning flights are not feasible in the study area for logistical reasons or when surveying east-exposed glaciers, the latter scenario should be considered.

In our pilot study, we covered part of the Forni glacier tongue, and only investigated hazards related to the glacier collapse. Our maps can help identify safer paths where mountaineers and skiers can visit the glacier and reach the most important summits. However, the increase in collapse structures owing to climate change requires multi-temporal monitoring. A comprehensive risk assessment should also cover the entire glacier, to investigate the probability of serac detachment and provide an estimate of the glacier mass balance with the geodetic method. While our integrated approach using a multicopter and terrestrial photogrammetry should be preferred to investigate small individual ice bodies, fixed-wing UAVs, ideally equipped with an RTK system and ability to tilt the camera off-nadir, might be the platform of choice to cover large distances (see e.g. Ryan et al., 2017), potentially reducing the number of flights and solving issues with GCP placement. Such platforms could help collect sufficient data for hazard management strategies up to the basin scale in Stelvio National Park and other sectors of the Italian Alps, eventually replacing aerial LiDAR surveys. Cost analyses (Matese et al., 2015) should also be performed to evaluate the benefits of improved spatial resolution and DEM accuracy of UAVs compared to aerial and satellite surveys and choose the best approach for individual cases.

7 Conclusions

In our study, we compared point clouds generated from UAV photogrammetry, close-range photogrammetry and TLS to assess their quality and evaluate the potential in mapping and describing glacier hazards such as ring faults and normal faults, by carrying out a specific campaign in summer 2016. In addition, we employed orthophotos and point clouds from a UAV survey conducted in 2014 to analyze the evolution of glacier hazards and a DEM from an aerial photogrammetric survey conducted in 2007 to investigate glacier thickness changes between 2014 and 2016. The main findings of our study include:

- UAVs and terrestrial photogrammetric surveys provide reliable performances in glacial environments, outperform TLS in terms of logistics and costs, and are more flexible in relation to meteorological conditions.

- UAV and terrestrial photogrammetric blocks can be easily integrated providing more information than individual techniques to help identify glacier hazards.
- UAV-based DEMs can be employed to estimate thickness changes but improvements are necessary in terms of area covered and accuracy to calculate the geodetic mass balance of large glaciers.
- The Forni Glacier is rapidly collapsing with an increase in ring faults size, providing evidence of climate change in the region.
- The glacier thinning rate increased owing to collapses to 5.20 ± 1.11 ma^{-1} between 2014 and 2016.

The maps produced from the combined analysis of UAV and terrestrial photogrammetric point clouds can be made available through GIS web portals of Stelvio National Park or Lombardy region (http://www.geoportale.regione.lombardia.it/). A permanent monitoring programme should be setup to help manage risk in the area, issuing warnings and assisting mountain guides in changing hiking and ski routes as needed. The analysis of glacier thickness changes suggests a feedback mechanism which should be further analysed, with higher thinning rates leading to increased occurrence of collapses, with additional release of meltwater. Glacier downwasting is also of relevance for risk management in the protected area, providing valuable data to assess the increased chance of rockfalls and to improve forecasts of glacier meltwater production.

While our test was conducted on one of the largest glaciers in the Italian Alps, the integrated photogrammetric approach is easily transferrable to similar sized and much smaller glaciers, where it would be able to provide a comprehensive assessment of hazards and mass balance and become useful in decision support systems for natural hazard management. In larger regions, UAVs hold the potential to become the platform of choice but their performances and cost-effectiveness compared to aerial and satellite surveys need to be further evaluated.

Competing interests

The authors declare that they have no conflict of interest.

Acknowledgements

This study was funded by DARAS, the department for autonomies and regional affairs of the presidency of the council of the Italian government. The authors acknowledge the central scientific committee of CAI (Club Alpino Italiano – Italian Alpine Club) and Levissima San Pellegrino S.P.A. for funding the UAV quadcopter. The authors also thank Stelvio Park Authority for the logistic support and for permitting the UAV surveys and IIT Regione Lombardia for the provision of the 2007 DEM. Acknowledgements also go to the GICARUS lab of Politecnico Milano at Lecco Campus for providing the survey equipment. Finally, the authors would also like to thank Tullio Feifer, Livio Piatta, and Andrea Grossoni for their help during field operations.

References

Abellán, A., Oppikofer, T., Jaboyedoff, M., Rosser, N. J., Lim, M. and Lato, M. J.: Terrestrial laser scanning of rock slope instabilities. Earth Surface Processes and Landforms, 39, 80–97, 2014, doi:10.1002/esp.3493.

Aicardi, I., Chiabrando, F.,Grasso, N., Lingua, A.M., Noardo, F. and Spanò, A.: UAV photogrammetry with oblique images: first analysis on data acquisition and processing, International Archives of the Photogrammetry, Remote Sensing and Spatial Information Sciences, XXIII ISPRS Congress, Prague, Czech Republic, 12–19 July 2016, 41-B1, 835-842, 2016, doi: 10.5194/isprs-archives-XLI-B1-835-2016.

Azzoni, R.S., Fugazza, D., Zennaro, M., Zucali, M., D'Agata, C., Maragno, D., Cernuschi, M., Smiraglia, C. and Diolaiuti, G.A.: Recent structural evolution of Forni Glacier tongue (Ortles-Cevedale Group, Central Italian Alps), submitted to Journal of Maps.

Berthier, E., Arnaud, Y., Kumar, R., Ahmad, S., Wagnon, P. and Chevallier, P.: Remote sensing estimates of glacier mass balances in the Himachal Pradesh (Western Himalaya, India), Remote Sensing of Environment, 108, 327-338, 2007, doi: 10.1016/j.rse.2006.11.017.

Berthier, E., Cabot, V., Vincent, C. and Six, D.: Decadal Region-Wide and Glacier-Wide Mass Balances Derived from Multi-Temporal ASTER Satellite Digital Elevation Models.Validation over the Mont-Blanc Area, Frontiers in Earth Science, 4, 63, 2016, doi: 10.3389/feart.2016.00063.

Bhardwaj, A., Sam, L., Akanksha, Martin-Torres, F.J. and Kumar, R.: UAVs as remote sensing platform in glaciology: Present applications and future prospects, Remote Sensing of Environment, 175, 196-204, 2016, doi: 10.1016/j.rse.2015.12.029.

Blasone, G., Cavalli, M. and Cazorzi, F.: Debris-Flow Monitoring and Geomorphic Change Detection Combining Laser Scanning and Fast Photogrammetric Surveys in the Moscardo Catchment (Eastern Italian Alps), in: Lollino, G., Arattano, M., Rinaldi, M., Giustolisi, O., Marechal, J.C. and Grant, G. (eds) Engineering Geology for Society and Territory, 3, Springer, Cham, 51-54, 2015, doi: 10.1007/978-3-319-09054-2_10.

Carey, M., McDowell, G., Huggel, C., Jackson, M., Portocarrero, C., Reynolds, J.M. and Vicuña, L.: Integrated approaches to adaptation and disaster risk reduction in dynamic sociocryospheric systems, in: Haeberli, W. and Whiteman, C. (Eds.), Snow and Ice-related Hazards, Risks and Disasters, Elsevier, 219-261, 2014, doi: 10.1016/B978-0-12-394849-6.00008-1.

Clague, J.: Glacier Hazards, in: Bobrowski, P. (Ed.), Encyclopedia of Natural Hazards, Springer, 400-405, 2013, doi: 10.1007/978-1-4020-4399-4_156.

Chiarle, M., Iannotti, S., Mortara, G. and Deline, P.: Recent debris flow occurrences associated with glaciers in the Alps, Global and Planetary Change, 56, 123-136, 2007, doi: 10.1016/j.gloplacha.2006.07.003.

Colomina, I. and Molina, P.: Unmanned aerial systems for photogrammetry and remote sensing: A review, ISPRS Journal of Photogrammetry and Remote Sensing, 92, 79-97, 2014, doi: 10.1016/j.isprsjprs.2014.02.013.

D'Agata, C., Bocchiola, D., Maragno, D., Smiraglia, C. and Diolaiuti, G.A.: Glacier shrinkage driven by climate change during half a century (1954–2007) in the Ortles-Cevedale group (Stelvio National Park, Lombardy, Italian Alps), Theoretical and Applied Cimatology, 116, 169-190, 2014, doi: 10.1007/s00704-013-0938-5.

Dewez, T.J.B., Leroux, J. and Morelli, S.: Cliff collapse hazard from repeated multicopter UAV acquisitions: return on experience, The International Archives of the Photogrammetry, Remote Sensing and Spatial Information Sciences, XXIII ISPRS Congress, Prague, Czech Republic, 12–19 July 2016, 41-B5, 805-811, 2016, doi: 10.5194/isprs-archives-XLI-B5-805-2016

Diolaiuti, G.A. and Smiraglia, C.: Changing glaciers in a changing climate: how vanishing geomorphosites have been driving deep changes in mountain landscapes and environments, Géomorphologie : Relief, Processus, Environnement, 2, 131-152, 2010, doi: 10.4000/geomorphologie.7882.

Diolaiuti, G.A., Bocchiola, D., D'Agata, C. and Smiraglia, C.: Evidence of climate change impact upon glaciers' recession within the Italian Alps, Theoretical and Applied Climatology, 109,429-445, 2012, doi: 10.1007/s00704-012-0589-y

Eltner, A., Kaiser, A., Castillo, C., Rock, G., Neugirg, F. and Abellán, A.: Image-based surface reconstruction in geomorphometry – merits, limits and developments. Earth Surface Dynamics, 4, 359-389, 2016, doi: 10.5194/esurf-4-359-2016.

Fioletti, M., Bonetti, M., Smiraglia, C., Diolaiuti, G.A., Breganze, C., dal Toso, M. and Facco, L.: Indagini radar per lo studio delle caratteristiche endoglaciali del ghiacciaio dei Forni in alta Valtellina, Neve e Valanghe, 87, 40-45, 2016

Fischer, M., Huss, M., Barboux, C. and Hoelzle, M.: The new Swiss Glacier Inventory SGI2010: relevance of using high-resolution source data in areas dominated by very small glaciers, Arctic, Antarctic and Alpine Research, 46,933-945, 2014, doi: 10.1657/1938-4246-46.4.933.

Fischer, M., Huss, M. and Hoelzle, M.: Surface elevation and mass changes of all Swiss glaciers 1980–2010, The Cryosphere, 9, 525-540, 2015, doi: 10.5194/tc-9-525-2015

Forlani, G., Pinto, L., Roncella, R. and Pagliari, D.: Terrestrial photogrammetry without ground control points, Earth Science Informatics, 7, 71-81, 2014, doi: 10.1007/s12145-013-0127-1.

Fugazza, D., Senese, A., Azzoni, R.S., Smiraglia, C., Cernuschi, M., Severi, D. and Diolaiuti, G.A.: High-resolution mapping of glacier surface features. The UAV survey of the Forni glacier (Stelvio national park, Italy), Geografia Fisica e Dinamica Quaternaria, 38, 25-33, 2015, doi: 10.4461/GFDQ.2015.38.03.

Furukawa, Y. and Ponce, J.: Accurate Camera Calibration from Multi-View Stereo and Bundle Adjustment, International Journal of Computer Vision, 84, 257–268, 2009, doi: 10.1007/s11263-009-0232-2.

Garavaglia, V., Diolaiuti, G.A., Smiraglia, C., Pasquale, V. and Pelfini, M.: Evaluating Tourist Perception of Environmental Changes as a Contribution to Managing Natural Resources in Glacierized areas: A Case Study of the Forni Glacier (Stelvio National Park, Italian Alps), Environmental Management, 50, 1125-1138, 2012, doi: 10.1007/s00267-012-9948-9.

Gagliardini, O., Gillet-Chaulet, F., Durand, G., Vincent, C. and Duval, P.: Estimating the risk of glacier cavity collapse during artificial drainage: The case of Tête Rousse Glacier, Geophysical Research Letters, 38, L10505, 2011, doi:10.1029/2011GL047536.

Gardent, M., Rabatel, A., Dedieu, J.-P., Deline, P.: Multitemporal glacier inventory of the French Alps from the late 1960s to the late 2000s, Global and Planetary Change, 120, 24-37, 2014. doi: 10.1016/j.gloplacha.2014.05.004.

Gindraux, S., Boesch, R. and Farinotti, D.: Accuracy Assessment of Digital Surface Models from Unmanned Aerial Vehicles' Imagery on Glaciers, Remote sensing, 9, 186, 2-15, 2017, doi:10.3390/rs9020186.

Gobiet, A., Kotlarski, S., Beniston, M., Heinrich, G., Rajczak, J., Stoffel, M.: 21st century climate change in the European Alps—A review, Science of The Total Environment, 493, 1138-1151, 2014, doi: 10.1016/j.scitotenv.2013.07.050.

Harris, C., Arenson, L.U., Christiansen, H.H., Etzelmueller, B., Frauenfelder, R., Gruber, S., Haeberli, W., Hauck, C., Hoelzle, M., Humlum, O., Isaksen, K., Kaab, A., Kern-Luetschg, M., Lehning, M., Matsuoka, N., Murton, J.B., Noetzli, J., Phillips, M., Ross, N., Seppaelae, M., Springman, S.M. and Vonder Muehll, D.: Permafrost and climate in Europe: Monitoring and modelling thermal, geomorphological and geotechnical responses, Earth-Science Reviews, 92, 117-171, 2009, doi: 10.1016/j.earscirev.2008.12.002.

Hoffmann-Wellenhof, B., Lichtenegger, H. and Wasle, E.: GNSS – GPS, GLONASS, Galileo & more, Springer, 2008, doi: 10.1007/978-3-211-73017-1.

Howat, I.M., Smith, B.E., Joughin, I. and Scambos, T.A.: Rates of southeast Greenland ice volume loss from combined ICESat and ASTER observations, Geophysical Research Letters, 35, L17505, 2008, doi:10.1029/2008GL034496.

Immerzeel, W.W., Kraaijenbrink, P.D.A., Shea, J.M., Shrestha, A.B., Pellicciotti, F., Bierkens, M.F.P. and de Jong, S.M.: High-resolution monitoring of Himalayan glacier dynamics using unmanned aerial vehicles, Remote Sensing of Environment, 150,93-103, 2014, doi: 10.1016/j.rse.2014.04.025.

Jokinen, O. and Geist T.: Accuracy aspects in topographical change detection of glacier surface, in: Remote sensing of glaciers, CRC Press/Balkema, Leiden, the Netherlands, 269-283, 2010, doi: 10.1201/b10155-15.

Kaab, A., Huggel., C., Fischer, L., Guex, S. Paul, F., Roer., I., Salzmann, N., Schlaefli, S., Schmutz, K., Schneider, D., Strozzi, T. and Weidmann, Y.: Remote sensing of glacier- and permafrost-related hazards in high mountains: an overview, Natural Hazards and Earth System Sciences, 5, 527–554, 2005a, doi: 10.5194/nhess-5-527-2005.

Kaab, A., Reynolds, J.M. and Haeberli, W.: Glacier and Permafrost hazards in high mountains, in: Huber U.M., Bugmann H.K.M., Reasoner M.A. (eds) Global Change and Mountain Regions. Advances in Global Change Research, Springer, Dordrecht, 225-234, 2005b, doi: 10.1007/1-4020-3508-X_23.

Kaufmann, V. and Ladstädter, R.: Application of terrestrial photogrammetry for glacier monitoring in Alpine environments, International Archives of the Photogrammetry, Remote Sensing and Spatial Information Sciences, Beijing, China, 37-B8, 813-818, 2008.

Kaufmann, V. and Seier, G.: Long-term monitoring of glacier change at Gössnitzkees (Austria) using terrestrial photogrammetry, The International Archives of the Photogrammetry, Remote Sensing and Spatial Information Sciences, XXIII ISPRS Congress, Prague, Czech Republic, 12-19 July 2016, 41-B8, 495-502, 2016, doi: 10.5194/isprs-archives-XLI-B8-495-2016

Keiler, M., Knight, J. and Harrison, S.: Climate change and geomorphological hazards in the eastern European Alps, Philosophical Transactions of The Royal Society A, 368, 2461–2479, 2010, doi: 10.1098/rsta.2010.0047.

Kellerer-Pirklbauer, A., Bauer, A. and Proske, H.: Terrestrial laser scanning for glacier monitoring: Glaciation changes of the Gößnitzkees glacier (Schober group, Austria) between 2000 and 2004, 3rd Symposion of the Hohe Tauern National Park for research in protected areas, castle of Kaprun, Austria, 15-17 September 2005, 97-106, 2005.

Lague, D., Brodu, N., Leroux, J.: Accurate 3D comparison of complex topography with terrestrial laser scanner: application to the Rangitikei canyon (N-Z). Journal of Photogrammetry and Remote Sensing, 82, 10–26, 2013, doi:10.1016/j.isprsjprs.2013.04.009.

Matese, A., Toscano, P., Di Gennaro, S.F., Genesio, L., Vaccari, F.P., Primicerio, J., Belli, C., Zaldei, A., Bianconi, R., Gioli, B.: Intercomparison of UAV, Aircraft and Satellite Remote Sensing Platforms for Precision Viticulture, Remote Sensing, 7, 2971-2990, 2015, doi:10.3390/rs70302971.

Mugnier, C.J.: Grids & Datum. Italian Republic. Photogrammetric Engineering and Remote Sensing, 71, 889-890, 2005.

Nuth, C. and Kaab, A.: Co-registration and bias corrections of satellite elevation data sets for quantifying glacier thickness change, The Cryosphere, 5, 271-290, 2011, doi: 10.5194/tc-5-271-2011.

Oborne, M.: Mission planner software. Available at: http://ardupilot.org/planner/, last access: 18/05/2017, 2013.

O'Connor, J., Smith, M.J. and James, M.R.: Cameras and settings for aerial surveys in the geosciences: optimising image data, Progress in Physical Geography, 41, 1-20, 2017, doi: 10.1177/0309133317703092.

Palomo, I.: Climate Change Impacts on Ecosystem Services in High Mountain Areas: A Literature Review, Mountain Research and Development, 37,179-187, 2017, doi: 10.1659/MRD-JOURNAL-D-16-00110.1.

Piermattei, L., Carturan, L. and Guarnieri, A.: Use of terrestrial photogrammetry based on structure from motion for mass balance estimation of a small glacier in the Italian Alps. Earth Surface Processes and Landforms, 40, 1791-1802, 2015, doi: 10.1002/esp.3756.

Piermattei, L., Carturan, L., de Blasi, F., Tarolli, P., Dalla Fontana, G., Vettore, A. and Pfeifer, N.: Suitability of ground-based SfM–MVS for monitoring glacial and periglacial processes, Earth Surface Dynamics, 4, 325-443, 2016, doi: 10.5194/esurf-4-425-2016.

Pomerleau, F., Colas, F., Siegwart, R. and Magnenat, S.: Comparing ICP variants on real world data sets. Autonomous Robots, 34, 133–148, 2013, doi: 10.1007/s10514-013-9327-2.

Quincey, D.J., Lucas, R.M., Richardson. S.D., Glasser, N.F., Hambrey, N.J. and Reynolds, J.M.: Optical remote sensing techniques in high-mountain environments: application to glacial hazards, Progress in Physical Geography, 29, 475-505, 2005, doi: 10.1191/0309133305pp456ra.

Riccardi, A. Vassena, G., Scotti, R., Sgrenzaroli, M.: Recent evolution of the punta S.Matteo serac (Ortles-Cevedale Group, Italian Alps), Geografia Fisica e Dinamica Quaternaria, 33, 215-219, 2010.

Rounce, D.R., Watson, C.S. and McKinney, D.C.: Identification of Hazard and Risk for Glacial Lakes in the Nepal Himalaya Using Satellite Imagery from 2000–2015, Remote Sensing, 9, 654, 2017, doi:10.3390/rs9070654.

Ryan, J.C., Hubbard, A., Box, J.E., Brough, S., Cameron, K., Cook, J.M., Cooper, M., Doyle, S.H., Edwards, A., Holt, T., Irvine-Fynn, T., Jones, C., Pitcher, L.H., Rennermalm, A.K., Smith, L.C, Stibal,

M. and Snooke, N.: Derivation of High Spatial Resolution Albedo from UAV Digital Imagery: Application over the Greenland Ice Sheet, Frontiers in Earth Science, 5, 40, 2017, doi: 10.3389/feart.2017.00040.

Seier, G., Kellerer-Pirklbauer, A., Wecht, M., Hirschmann, S., Kaufmann, V., Lieb, G.K. and Sulzer, W.: UAS-Based Change Detection of the Glacial and Proglacial Transition Zone at Pasterze Glacier, Austria. Remote Sensing, 9, 549, 2017, doi:10.3390/rs9060549.

Senese, A., Diolaiuti, G.A., Mihalcea, C. and Smiraglia, C.: Energy and Mass Balance of Forni Glacier (Stelvio National Park, Italian Alps) from a Four-Year Meteorological Data Record, Arctic, Antarctic and Alpine Research, 44, 122-134, 2012, doi: 10.1657/1938-4246-44.1.122.

Smiraglia, C., Azzoni, R.S., D'Agata, C., Maragno, D., Fugazza, D. and Diolaiuti, G.A.: The evolution of the Italian glaciers from the previous data base to the new Italian inventory. Preliminary considerations and results, Geogr. Fis. Dinam. Quat., 38, 79-87, 2015, doi: 10.4461/GFDQ.2015.38.08.

Spetsakis, M. and Aloimonos, J.Y.: A multi-frame approach to visual motion perception, International Journal of Computer Vision, 6, 245-255, 1991, doi: 10.1007/BF00115698.

Teunissen, P.J.G.: Testing theory. An introduction. Series on Mathematical Geodesy and Positioning, VSSD Delft, The Netherlands, 2009.

Urbini, S., Zirizzotti, A., Baskaradas, J.A., Tabacco, I.E., Cafarella, L., Senese, A., Smiraglia, C., Diolaiuti, G.: Airborne radio echo sounding (RES) measures on alpine glaciers to evaluate ice thickness and bedrock geometry: Preliminary results from pilot tests performed in the ortles-cevedale group (Italian alps), Annals of Geophysics, 60, G0226, doi: 10.4401/ag-7122, 2017.

Vincent, C., Thibert, E., Harter, M., Soruco, A. and Gilbert, A.: Volume and frequency of ice avalanches from Taconnaz hanging glacier, French Alps, Annals of Glaciology, 56, 17-25, 2015, doi: 10.3189/2015AoG70A017.

Westoby, M.J., Brasington, J., Glasser, N.F., Hambrey, M.J. and Reynolds, J.M.: Structure-from-Motion' photogrammetry: A low-cost, effective tool for geoscience applications, Geomorphology, 179, 300-314, 2012, doi: 10.1016/j.geomorph.2012.08.021.

Winkler, M., Pfeffer, W.T. and Hanke, K.: Kilimanjaro ice cliff monitoring with close range photogrammetry, International Archives of the Photogrammetry, Remote Sensing and Spatial Information Sciences, XXII ISPRS Congress, Melbourne, Australia, 25 August-1 September 2012, 39-B5, 441-446, 2012.

Tables

DEM pair	Elevation differences without co-registration shifts ($\mu_{\Delta H} \pm \sigma_{\Delta H}$) [m]	Co-registration shifts		Elevation differences with co-registration shifts ($\mu_{\Delta H} \pm \sigma_{\Delta H}$) [m]
		X [m]	Y [m]	
2007-2014	1.96±2.60	1.11	-1.11	0.00±1.70
2007-2016	-0.43±3.48	2.44	-1.11	0.00±2.60
2014-2016	-2.92±3.21	-0.20	-1.30	0.00±2.22

Table 1: Statistics of the elevation differences between DEM pairs before and after the application of co-registration shifts.

Sample Window	Area (m^2)	number of points in sample windows			Mean and standard deviation of point density [points/m^2]			Number of point above the lower 12.5% percentile		
		UAV photogramm.	Terrestrial Photogramm.	TLS	UAV Photogramm.	Terrestrial Photogramm.	TLS	UAV Photogramm.	Terrestrial Photogramm.	TLS
1	2793	-	1984k	141k	-	1654±637	226±100	-	880	26
2	1806	76k	2175k	130k	109±29	2297±708	391±217	61	881	0
3	495	43k	712k	25k	103±27	1978±606	151±60	49	766	31
4	672	62k	557k	33k	108±22	1384±530	141±69	62	324	2
5	3960	406k	810k	-	141±22	485±227	-	97	31	-

Table 2: Area and number of points in each sample window on the Forni Glacier terminus, mean and standard deviation of local point density and number of points above the lower 12.5% percentile in each window.

Sample Window		Means and Std. Dev.s of M3C2 distances [cm]			RMSE of M3C2 distances [cm]		
	Ref.	TLS	TLS	UAV Photogramm.	TLS	TLS	UAV Photogramm.
	Slave	Terrestrial Photogramm.	UAV Photogramm.	Terrestrial Photogramm.	Terrestrial Photogramm.	UAV Photogramm.	Terrestrial Photogramm.
1		4.5±7.4	-	-	8.7	-	-
2		-1.1±10.5	14.8±34.7	-14.5±26.7	10.6	37.7	30.4
3		8.4±4.1	14.7±15.1	-8.5±18.9	9.4	21.1	20.7
4		2.8±5.3	9.4±22.2	-2.3±24.9	6.0	24.0	25.0
5		-	-	-8.5±25.3	-	-	26.7

Table 3: Statistics on distances between point

clouds computed on the basis of M3C2 algorithm.

DEM pair	Mean thickness change [m]	Mean thinning rates [ma^{-1}]	Volume Change [10^6 m^3]
2007-2014	-31.91 ± 1.70	-4.55 ± 0.24	-10.00 ± 0.12
2007-2016	-42.86 ± 2.60	-4.76 ± 0.29	-13.46 ± 0.14
2014-2016	-10.41 ± 2.22	-5.20 ± 1.11	-3.29 ± 0.05

Table 4: Average ice thickness change, thinning rates and volume loss from DEM differencing over a common reference area of 0.32 km^2 for all DEM pairs. Uncertainty of thickness change expressed as 1σ of residual elevation differences over stable areas after DEM co-registration.

Figures

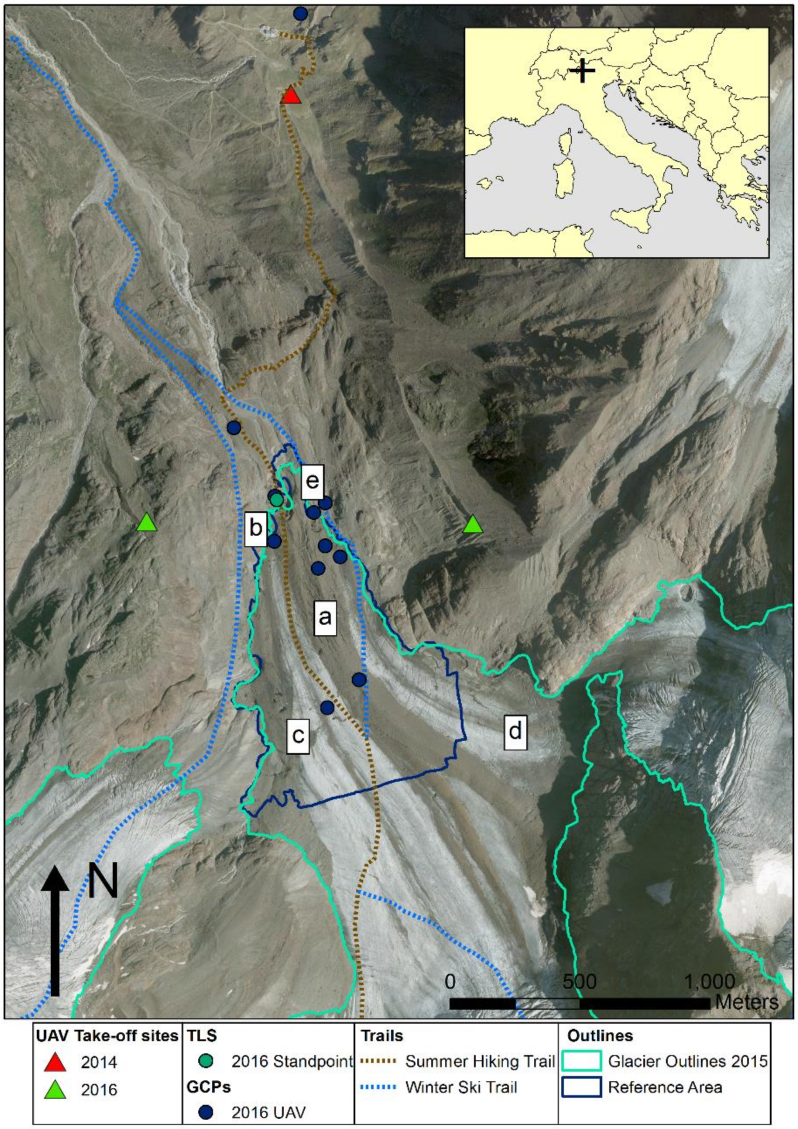

Figure 1: the tongue of Forni Glacier. The map shows the location of take-off/landing sites for the 2014 and 2016 UAV surveys (in 2016 two different landing sites were used), standpoint of TLS survey, GCPs used in the UAV photogrammetry surveys and trails crossing the glaciers. Letters a-e identify the location of features described in Fig.2. Base map from 2015 courtesy of IIT Regione Lombardia WMS Service. Trails from Kompass online cartography at https://www.kompass-italia.it/info/mappa-online/.

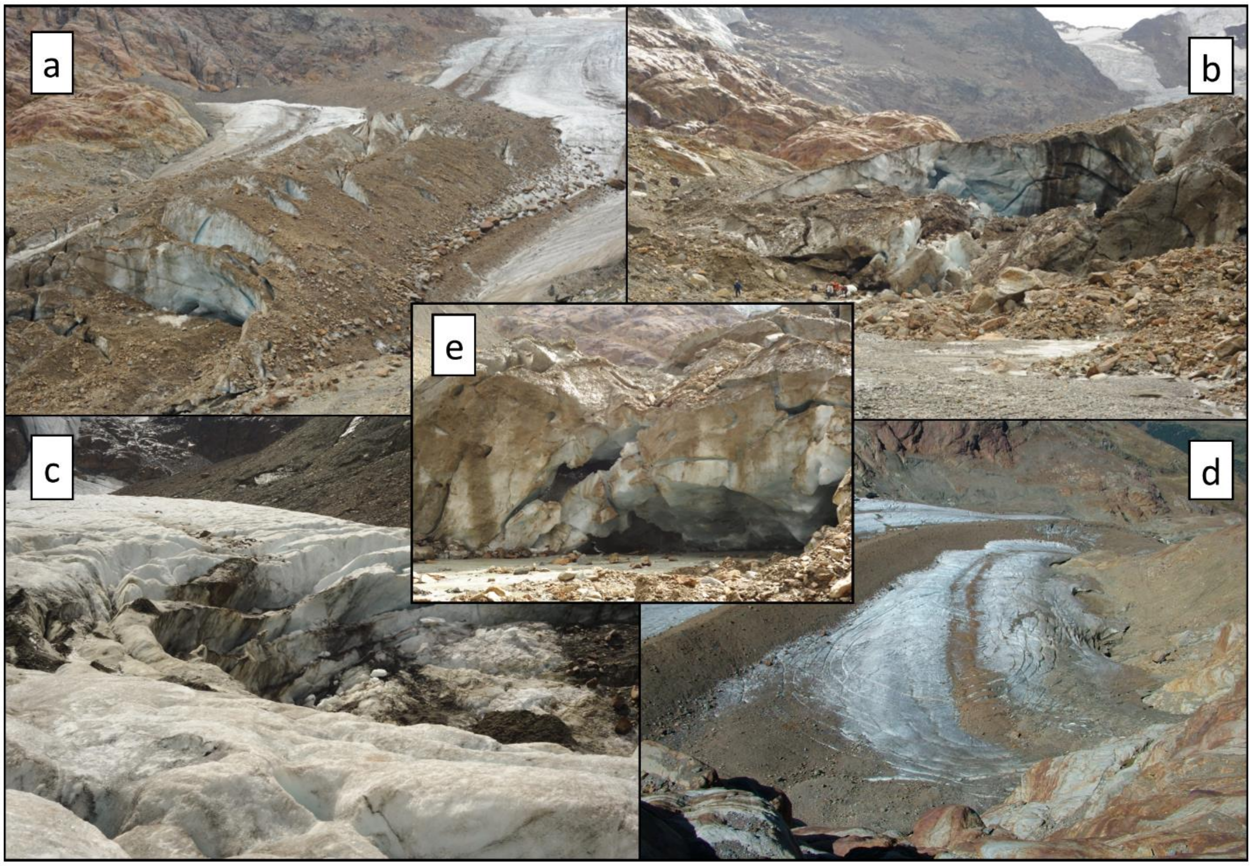

Figure 2: Collapsing areas on the tongue of Forni Glacier. (a) Faults cutting across the eastern medial moraine; (b) glacier terminus; (c) Near-circular collapsed area on the central tongue; (d) Large ring fault on the eastern tongue at the base of the icefall. Photo courtesy of G.Cola; (e) Close-up of a vertical ice cliff at the glacier terminus. The location of features is reported in Fig.1

Aircraft type	Swinglet CAM, Commercial platform
Digital Camera	Canon Ixus 127 HS
Camera technical features	16 Megapixel, focal length 4.3 mm
GNSS antenna	GPS only
Weight (incl. payload)	0.50 Kg
Battery time	30 minutes

Aircraft type	Customized, with Tarot frame 650 size, VR Brain 5.2 Autopilot & APM Arducopter 3.2.1 Firmware
Digital camera	Canon Powershot ELPH 320 HS
Camera technical features	16 Megapixel, focal length 4.3 mm
GNSS antenna	GPS+GLONASS (Galileo compatible)
Weight (incl. pay-load)	2.75 Kg
Battery time	20-25 minutes

Figure 3: The UAVs used in surveys of the Forni Glacier and their characteristics. (a) The SwingletCam fixed-wing aircraft employed in 2014, at its take off site by Lake Rosole; (b) The customized quadcopter used in 2016 in the lab.

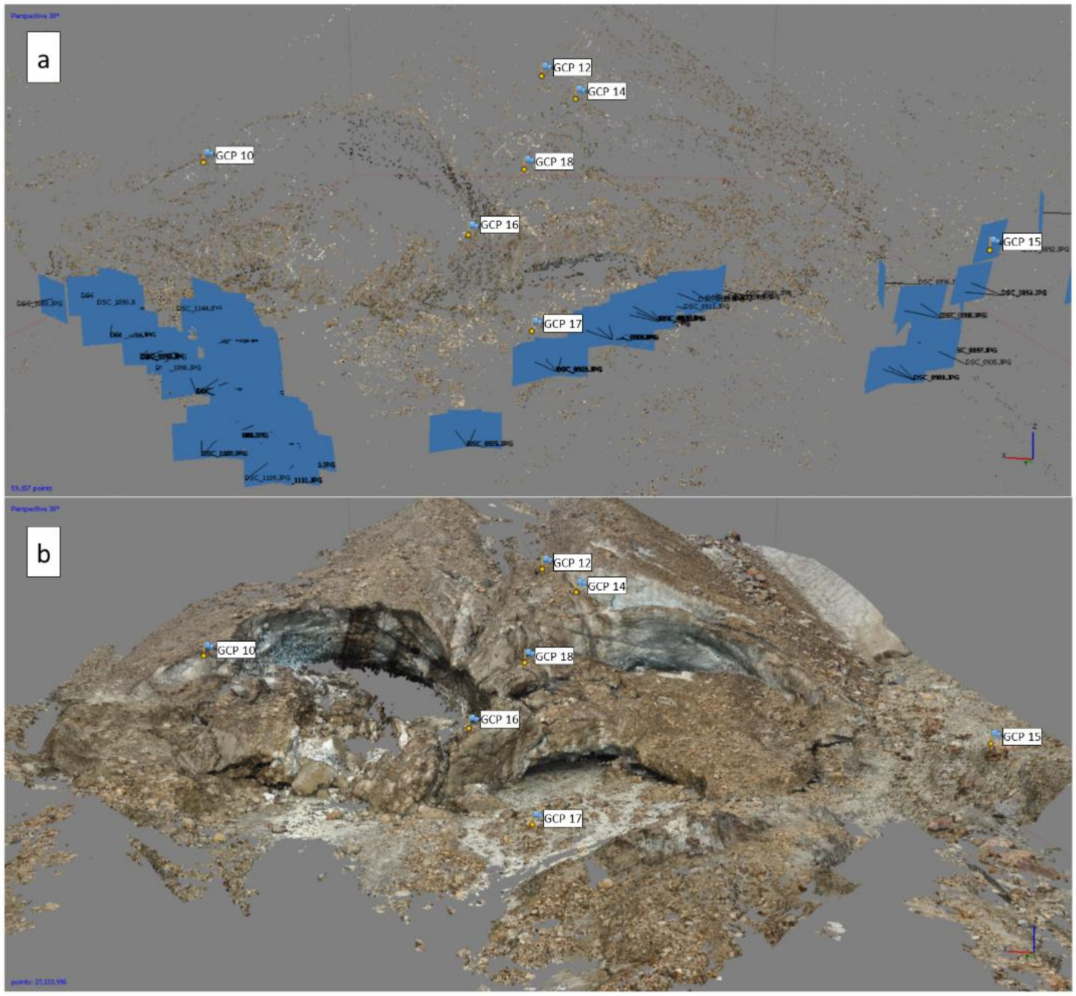

Figure 4: 3D reconstruction of the glacier terminus from the terrestrial photogrammetric survey of 2016 : (a) locations of camera stations in front of the glacier and 3D coordinates of tie points extracted during SfM for image orientation; (b) point cloud of the glacier terminus with positions of GCPs.

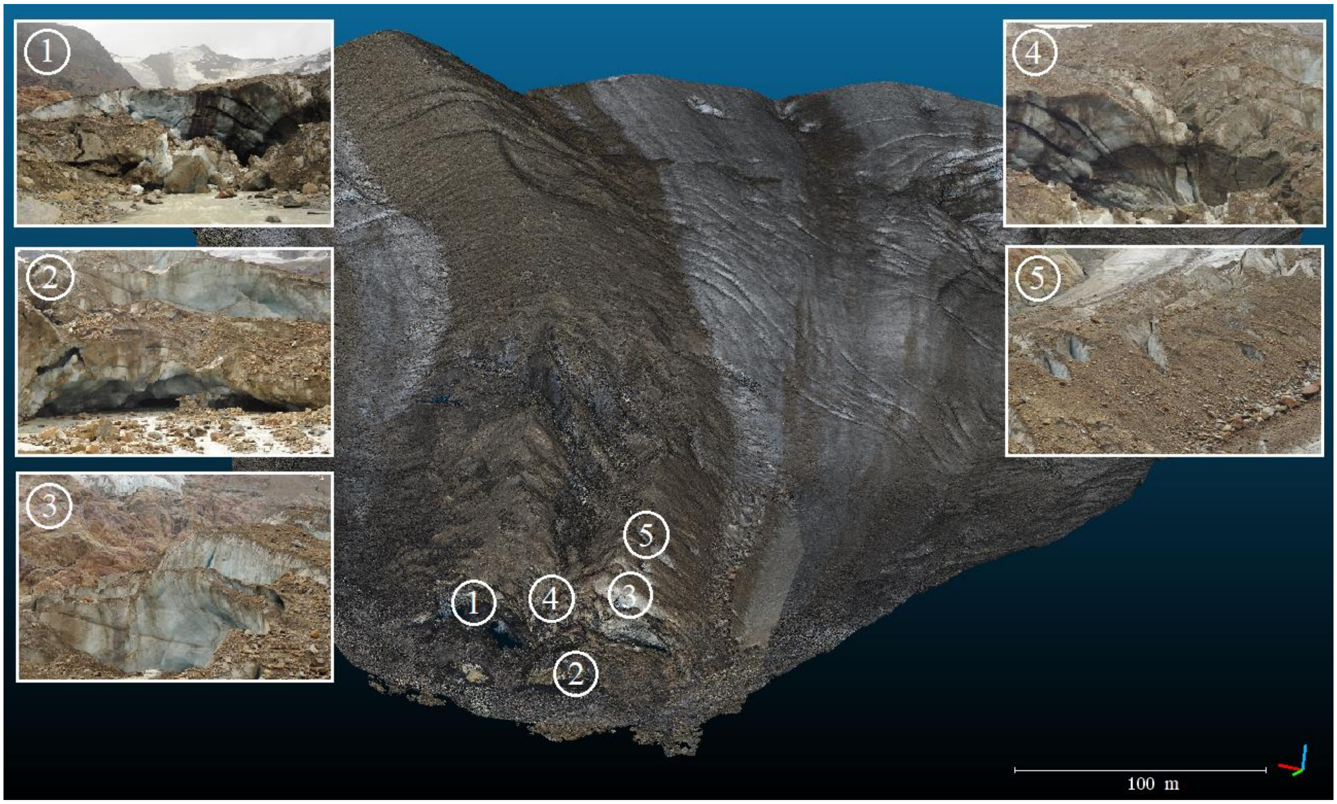

Figure 5: Location of different glacier features or hazard-prone areas on the tongue of Forni glacier were the point cloud comparison was performed. The background image is the merged point cloud generated from the 2016 UAV and terrestrial photogrammetry survey.

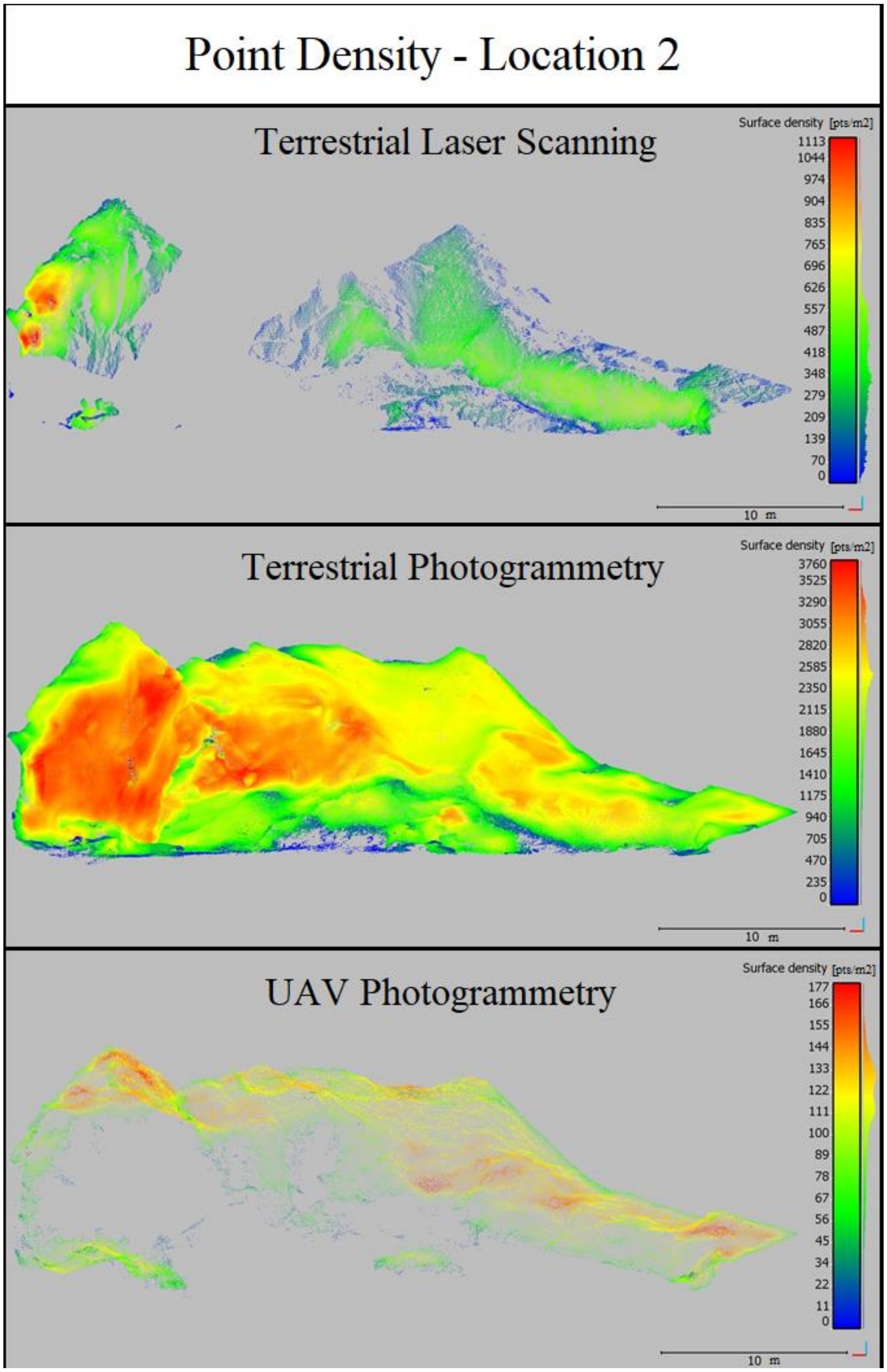

Figure 6: Maps of point density in sample location 2.

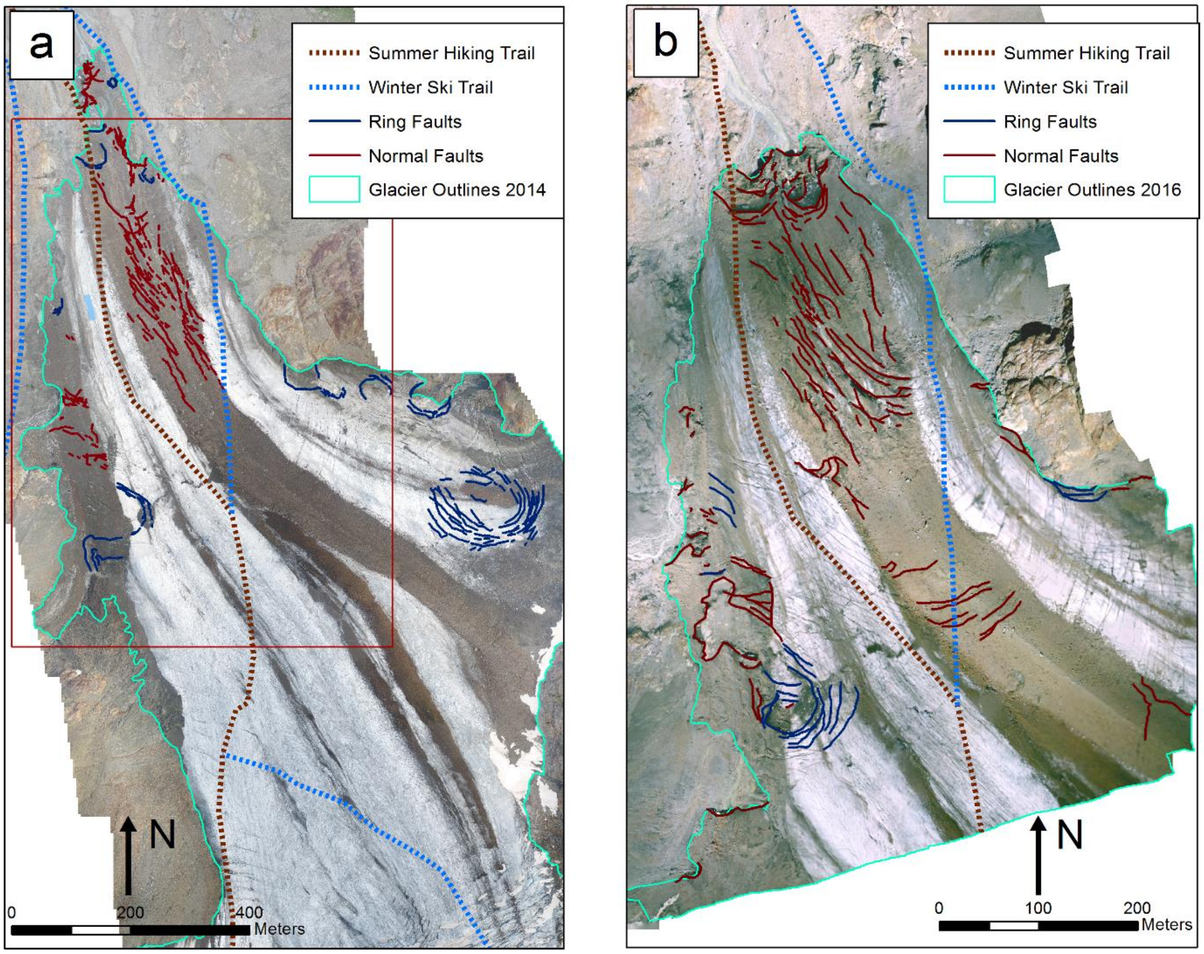

Figure 7: location of collapse structures, i.e. normal faults and ring faults and trails crossing the Forni Glacier (a) 2014, with 2014 UAV ortophoto as basemap. The red box marks the area surveyed in 2016. (b) 2016, with 2016 UAV orthophoto as basemap.Trails from Kompass online cartography at https://www.kompass-italia.it/info/mappa-online/.

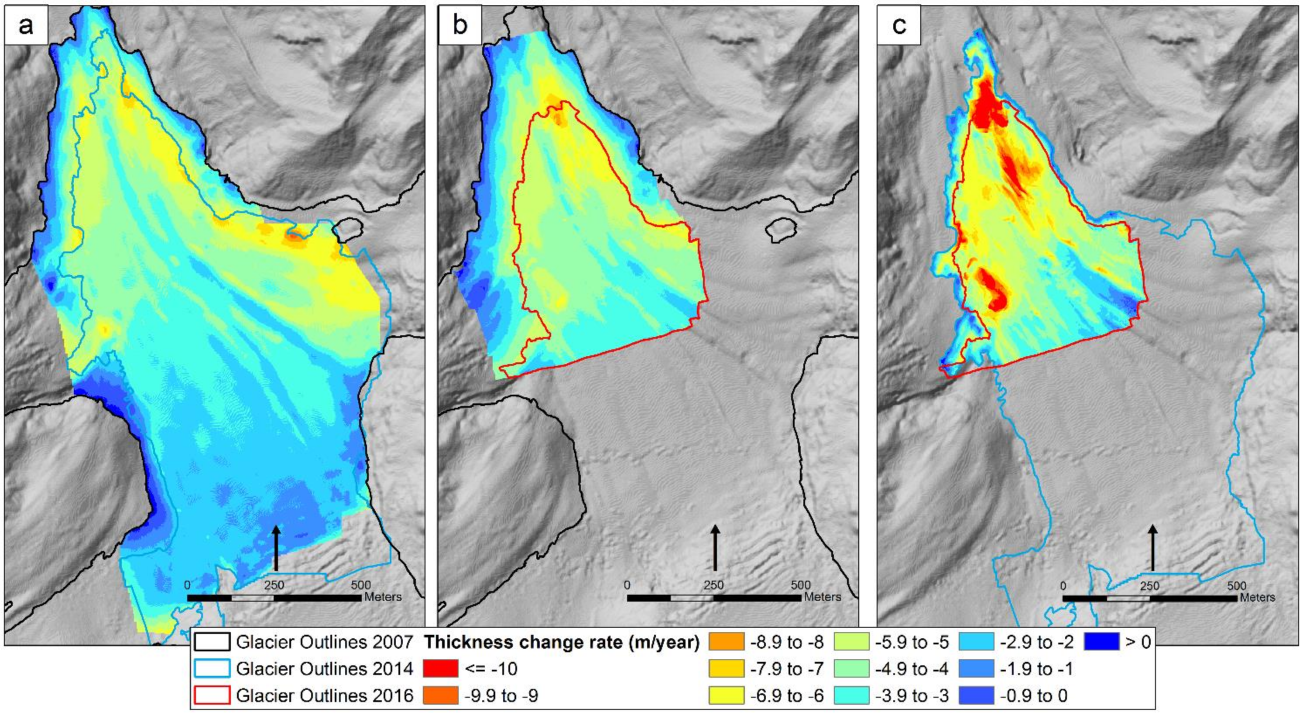

Figure 8: Ice thickness change rates from DEM differencing over (a) 2007-2014; (b) 2007-2016; (c) 2014-2016. Glacier outlines from 2014 and 2016 are limited to the area surveyed during the UAV campaigns. Base map from hillshading of 2007 DEM.